THE JOURNAL OF PHYSICAL CHEMISTRY LETTERS
A JOURNAL OF THE AMERICAN CHEMICAL SOCIETY

pubs.acs.org/JPCL Letter

Magnetic Field Alignment and Optical Anisotropy of MoS_2 Nanosheets Dispersed in a Liquid Crystal Polymer

Uri R. Gabinet, Changyeon Lee, Na Kyung Kim, Martin Hulman, Sarah M. Thompson, Cherie R. Kagan, and Chinedum O. Osuji*

Cite This: *J. Phys. Chem. Lett.* 2022, 13, 7994–8001 Read Online

ACCESS | Metrics & More | Article Recommendations | Supporting Information

ABSTRACT: Molybdenum disulfide (MoS_2) nanosheets exhibit anisotropic optical and electronic properties, stemming from their shape and electronic structure. Unveiling this anisotropy for study and usage in materials and devices requires the ability to control the orientation of dispersed nanosheets, but to date this has proved a challenging proposition. Here, we demonstrate magnetic field driven alignment of MoS_2 nanosheets in a liquid crystal (LC) polymer and unveil the optical properties of the resulting anisotropic assembly. Nanosheet optical anisotropy is observed spectroscopically by Raman and direction-dependent photoluminescence (PL) measurements. Resulting data indicate significantly lower PL emission due to optical excitation with electric field oscillation out of plane, parallel to the MoS_2 *c*-axis, than that associated with perpendicular excitation, with the dichroic ratio $I_{perp}/I_{par} = 3$. The approach developed here provides a useful route to elucidate anisotropic optical properties of MoS_2 nanosheets and to utilize such properties in new materials and devices.

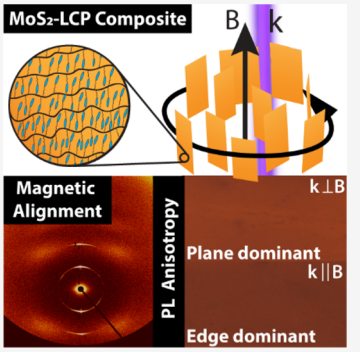

Atomically thin molybdenum disulfide (MoS_2) has attracted significant interest due to its electronic, optical, catalytic, and mechanical properties, some of which are not found, or are appreciably different, in the bulk material.[1−4] The mismatch between the strong intralayer covalent bonds[5,6] and weak interlayer van der Waals interactions allows easy exfoliation and separation of the bulk material into few-layer nanosheets.[7−12] The resulting atomically thin sheets with colloidal-scale lateral dimensions exhibit anisotropic properties including differences in catalytic,[13,14] thermal,[15] and optical[16−18] activity between the sheet basal planes and edges.

Optical anisotropy in MoS_2 has been experimentally explored by near-field measurements that have resolved differences in the Raman response[16,19] and dielectric constants of nanosheet basal planes and edges.[16,17] The anisotropy stems from the inherent 2D morphology of the MoS_2 nanosheets, which has been previously observed by aligning the nanosheets in a parallel or transverse configuration with respect to the probing beam.[19−26]

Optical anisotropy in MoS_2 nanosheets can be significant, as was recently indicated in a report by Volkov and co-workers on the giant optical anisotropy in MoS_2 nanosheets, showcasing a large birefringence of $\Delta n = 3$ and $\Delta n = 1.5$ for visible and infrared (IR) light, respectively.[6] In addition, anisotropic optical effects in MoS_2 may be substrate-induced due to morphological effects[22−24] or crystallographically dictated symmetry breaking and defectivity.[27,28] Excitonic emission by MoS_2 nanosheets is of particular interest for optoelectronic devices. MoS_2 photoluminescence (PL) can be manipulated through defect engineering and plasmonic coupling. In addition, at low temperatures, MoS_2 functions as a quantum emitter. Surprisingly little is known, however, regarding PL anisotropy in MoS_2, whether from first-principles calculations or experimental measurements.

Despite the impetus to elucidate the anisotropic optical properties in few-layer MoS_2, current methods to do so are lacking in their ability to robustly control few-layer MoS_2 nanosheet orientation, inhibiting the opportunities to devise technologies that harness the difference in optical properties parallel and transverse to the nanosheets surface normal or to further explore and study the anisotropy in detail. As highlighted above, studies of anisotropic effects in MoS_2 rely on orientation control of grown or patterned *bulk* MoS_2 films or particles, which are then studied by using traditional spectroscopic characterization techniques,[13,20−23,26,28] but disregard few-layer nanosheets, whose anisotropic characteristics may vary considerably from the bulk material. Conversely, the study of *individually* exfoliated MoS_2 nanosheets has relied on near-field techniques that are challenging to leverage, particularly in statistically relevant scenarios.[6,16,17] Hence, the ability to suspend individual nanosheets and control their orientation in a suitable dielectric medium would enable important studies of PL and other optical anisotropies in MoS_2 with a versatility that has thus far been lacking. Such

Received: June 13, 2022
Accepted: August 5, 2022
Published: August 19, 2022

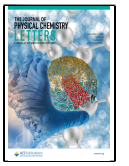

https://doi.org/10.1021/acs.jpclett.2c01819
J. Phys. Chem. Lett. 2022, 13, 7994–8001

an ability would also advance the prospects of harnessing these properties in applications of interest.

Here, we demonstrate an enabling technique to control the orientation of few-layer MoS_2 via the use of a liquid crystal polymer (LCP) to stably disperse individual and few-layer MoS_2 nanosheets with controlled orientation. This orientation control, in turn, allows the characterization of the optical anisotropic properties of such assemblies of nanosheets. We leverage magnetic-field-directed alignment of the LC director to control the nanosheet orientation as the two are coupled through the anchoring condition of the LC mesogens at the nanosheet surface (Figure 1).[29] The resulting aligned nanosheets in a LC polymer reveal the optical anisotropy of the MoS_2 and allow the use of traditional spectroscopic characterization to delineate basal plane versus edge contributions to optical signals in suspended few-layer MoS_2 nanosheets. We use the relative PL intensities from different incident light directions with respect to the magnetic field to estimate the edge and basal plane contributions to the emission. We anticipate that this approach to control the orientation of 2D-MoS_2 nanosheets can pave the way to further studies of the anisotropic properties (optical and others) of MoS_2 as well as the utilization of nanosheets in application and devices, which have been stymied by the current lack of techniques to robustly control the orientation of few-layer MoS_2.

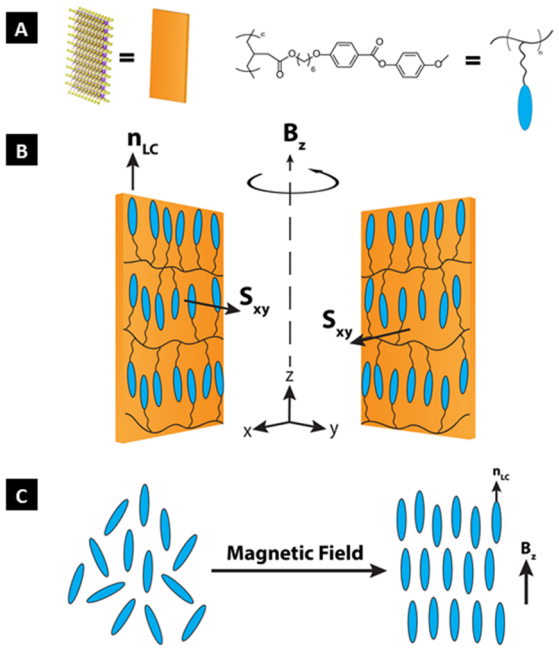

Figure 1. Schematic illustration depicting magnetic alignment of MoS_2 in a liquid crystal polymer (LCP). (A) Representation of MoS_2 nanosheets and chemical structure of polymerized RM105. (B) The nanosheets align with their surface normal perpendicular to the field direction. For a field applied along the *z*-axis ($\mathbf{B}_z$), this constrains the nanosheet surface normal to lie in the *xy*-plane ($\mathbf{S}_{xy}$) as depicted. This alignment results from the convolution of the planar anchoring of the mesogens (depicted as blue cigar-shaped objects) at the MoS_2 basal plane. (C) RM105 mesogens align with the LC director, $\mathbf{n}_{LC}$, parallel to the applied field due to their positive magnetic anisotropy (polymer backbone omitted for clarity).

A nanocomposite of few-layer MoS_2 dispersed in a LCP, polymerized RM105 (Figure 1A), was prepared by liquid phase exfoliation of MoS_2 in the reactive mesogen RM105 and subsequent solvent removal and polymerization. Briefly, bulk MoS_2 powder was mixed and sonicated with a LC monomer under an inert atmosphere, with 1,2-dichlorobenzene (DCB) used as a solvent. After separation of unexfoliated material by centrifugation, a solution containing exfoliated few-layer MoS_2 was obtained (Figure 2A,B), which exhibited long-term stability. Following solution casting and addition of a photoinitiator, LCP-dispersed 2D-MoS_2 was obtained by photopolymerization under UV light, with a final MoS_2 concentration of 0.01 wt % (see the Supporting Information for detailed methods).

The resulting LCP contained dispersed few-layer MoS_2 nanosheets, as indicated by the green color of the composite, in stark contrast to the pale white-yellow color of the LCP in the absence of MoS_2 or the gray color of nonexfoliated bulk-MoS_2 dispersed in the LCP (see Figure S1). UV−vis and PL spectra show the two characteristic excitonic transitions of few-layer MoS_2, confirming the presence of 2D-MoS_2 semiconducting nanosheets (Figure 2C). Two characteristic PL peaks can be identified at ∼637 and ∼696 nm, corresponding to the B and A excitons identified in the absorption spectrum at ∼609 and ∼672 nm, respectively.[2,30] The relatively high intensity of the B excitonic peak may originate from defects in the nanosheet structure developed during the exfoliation process[31−33] or due to cavity-like interactions of the B exciton with the mesoscale structure of the LC matrix, as previously seen.[34−36] Beyond the high intensity of the B excitonic peak, we observe relatively large Stokes shifts of the excitonic transitions, with ∼90 and ∼60 meV for the B and A transitions, respectively, compared to ∼0 and ∼20 meV, respectively, observed in mechanically exfoliated MoS_2 flakes (Figures 2C and S2).[30,37]

Raman spectroscopy of the LCP-dispersed MoS_2 shows the characteristic E^1_{2g} and A_{1g} modes of MoS_2 (see Figure 2D). The frequency difference between these two Raman modes can be used to determine the number of layers of MoS_2 in the nanosheets.[38] The frequency difference for the LCP-dispersed MoS_2 was 25.0 ± 0.6 cm^{-1} (see Figure 2E), which is significantly smaller than the measured frequency difference for bulk MoS_2 powder (26.3 ± 0.3 6 cm^{-1}, Figure 2D) and is consistent with the presence of few-layer MoS_2 nanosheets in the LCP, similar to previous reports of exfoliation in the presence of organic species in DCB.[39] This indicates that photopolymerization did not lead to significant aggregation of MoS_2. It is important to note that the exact number of layers cannot directly be determined from the described measurement, as effects caused by the organic LCP surrounding the 2D sheets may shift the position of the two Raman modes in a nonsystematic manner. However, the frequency difference of the LCP-dispersed MoS_2 is sufficiently different than that of bulk MoS_2 that the existence of few-layer MoS_2 dispersed in the LCP is not in question, even if the average number of layers cannot be quantified more accurately.[29,40,41]

Polymerized RM105 forms a smectic LCP, with the rigid phenyl benzoate moieties arranged in layers.[42,43] Temperature-resolved small-angle X-ray scattering (SAXS) and differential scanning calorimetry (DSC) indicated Smectic A−Nematic and Nematic−Isotropic transitions at T_{Sm-N} = 85 °C and T_{NI} = 112 °C, respectively (see Figure S3). The magnetic susceptibility anisotropy of the RM105 mesogen is sufficient to allow magnetic field control of the LC director orientation at field strengths of a few tesla. To align the system, in a typical procedure the LCP is heated into its isotropic state above T_{NI}

https://doi.org/10.1021/acs.jpclett.2c01819
J. Phys. Chem. Lett. 2022, 13, 7994−8001

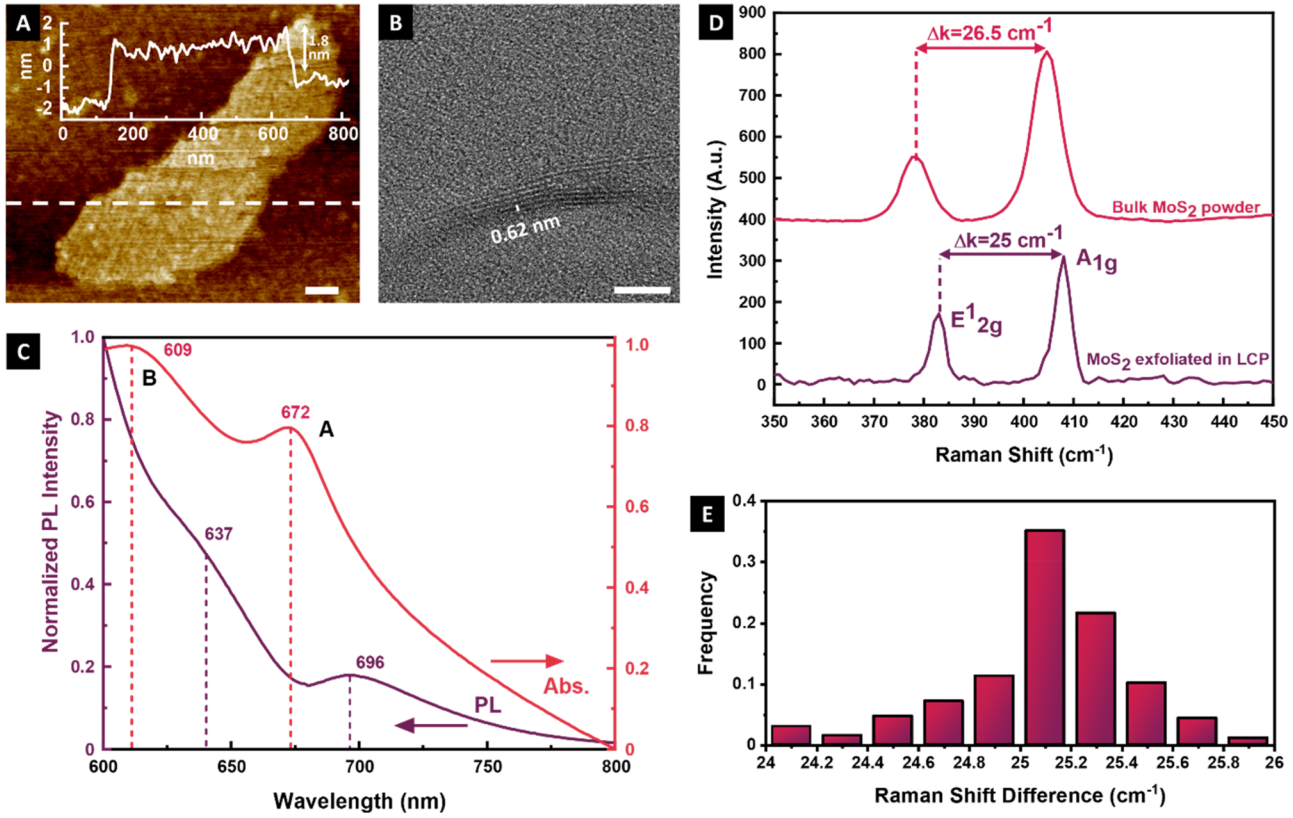

Figure 2. Characterization of few-layer MoS_2 nanosheets dispersed in the liquid crystal polymer (LCP). (A) AFM image of a single nanosheet, with a height profile along the marked dashed line. Scale bar represents 100 nm. (B) TEM image of nanosheet edges, showing each nanosheet is composed of ∼3−4 layers, with a single-layer thickness indicated. Scale bar represents 5 nm. (C) Normalized absorption (red) and PL spectra (purple) of the LCP-dispersed MoS_2, with absorption and PL bands, relating to the A and B excitonic transitions indicated. PL was measured under 532 nm excitation. (D) Raman spectra of the LCP-dispersed MoS_2 (purple) and the unexfoliated bulk MoS_2 powder (red), indicating the A_{1g} and E^1_{2g} Raman modes and their frequency difference. (E) Distribution of the A_{1g} and the E^1_{2g} Raman modes frequency difference in LCP-dispersed MoS_2.

(typically ∼130 °C) and then slowly cooled (∼0.1 °C/min) into the smectic state at room temperature in the presence of the field.

SAXS data from aligned and nonaligned samples are shown in Figure 3 with applied magnetic field directions as indicated (1D plots in Figures S3 and S4). The patterns from the field-processed samples (LCP and LCP with MoS_2) are anisotropic whereas those from samples not exposed to the magnetic field are isotropic. Three prominent features appear: (1) scattering concentrated along the meridional line, parallel to the field, at $q^1 = 2.55\ nm^{-1}$. This Bragg peak and its second- and third-order reflections originate from the smectic layer periodicity $d_{Sm} = 2\pi/q^1 = 2.5$ nm and alignment of the LC director parallel to the field. (2) Diffuse 4-fold scattering at $q^2 \sim 6\ nm^{-1}$, which can be attributed to undulations of the polymer backbone.[44] (3) Additional anisotropic scattering can be observed equatorially at the low-q region near the beamstop (Figure 3A,E). LCP samples that do not contain MoS_2 nanosheets do not display the same scattering in the low-q region as nanosheet containing LCP, indicating that this scattering originates from the MoS_2 nanosheets (see Figure 3B,D). Such "streaklike" scattering at low q is characteristically produced by sharp edges of colloidal-scale structures, for example as previously observed with lamellar organization of 2D clay[45,46] and graphene oxide[47] nanosheets. The orientation of the streak scattering along the equatorial line indicates a considerable population of MoS_2 nanosheets aligned with their surface normal perpendicular to the field. Direct TEM imaging of thin sections of magnetically aligned samples shows that the sheets are aligned in this manner, with their surface normal perpendicular to the magnetic field direction (Figure 3A, inset). Alignment is not observed when the sample is heated and cooled in the absence of the magnetic field (Figure 3C), as can be observed in the 2D SAXS plots as well as in the low-q region scattering intensity dependence on the azimuthal angle (Figure 3E).

Such alignment of the MoS_2 nanosheets is consistent with the expected planar anchoring behavior of the mesogenic side chains on the surface of MoS_2 as well as the alignment direction of the mesogenic units themselves with respect to the magnetic field. It is also consistent with previous reports on surface anchoring of mesogenic species affecting the magnetic alignment of planar inorganic particles.[48,49] Specifically, the LC director aligns parallel to the field direction, as seen from the concentration of scattered intensity from the smectic layers along the meridional line in the X-ray scattering data (Figure 3A,B). This reflects a positive value of the magnetic susceptibility anisotropy ($\Delta\chi > 0$) of the mesogens.[50,51] The planar anchoring of the mesogens at the nanosheet surface inferred by the sheet and director orientation has been observed previously in related mesogenic species on MoS_2.[29,52−55] This combination, of positive magnetic susceptibility in tandem with planar anchoring of the mesogenic units on the surface of MoS_2, leads directly to orientational

https://doi.org/10.1021/acs.jpclett.2c01819
J. Phys. Chem. Lett. 2022, 13, 7994−8001

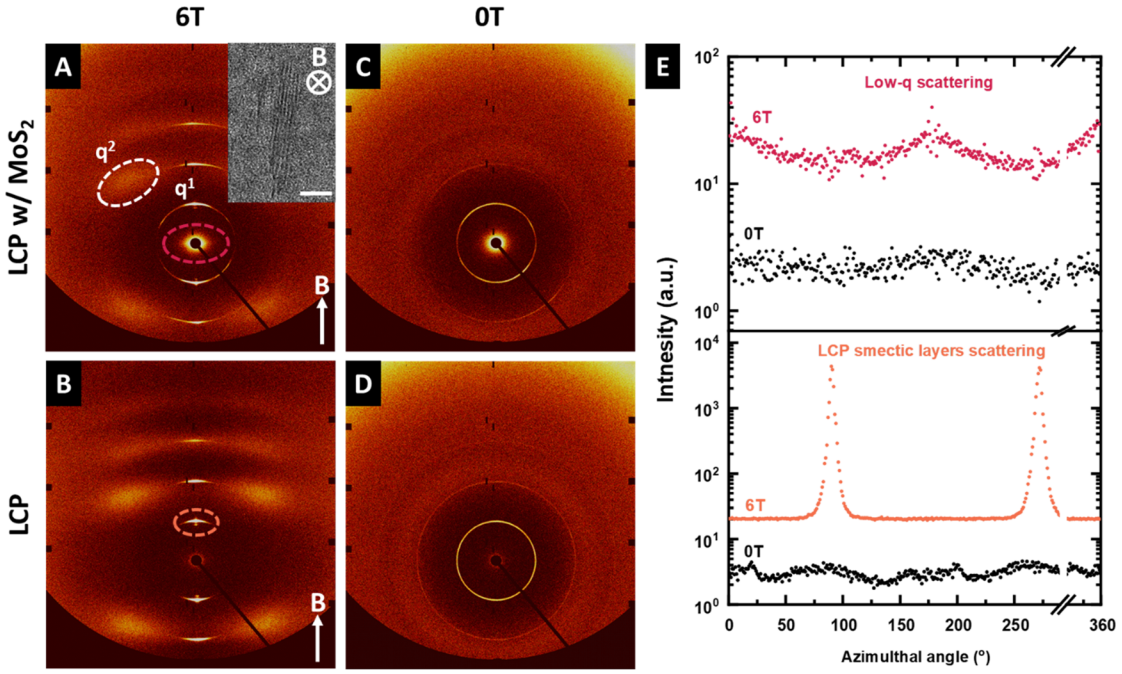

Figure 3. X-ray scattering from magnetic field aligned LCP dispersed−MoS_2 nanocomposite. (A) Scattering pattern of magnetically aligned MoS_2-containing LCP, with scattering from aligned smectic layer marked by q^1, polymer backbone undulation marked as q^2, and anisotropic scattering from MoS_2 marked in red. Field direction is an indicated. Inset: TEM micrograph of vertically aligned MoS_2 nanosheet embedded in an LCP matrix, following magnetic alignment. The magnetic field direction is out of plane, and the scale bar represents 5 nm. (B) Scattering pattern of magnetically aligned MoS_2-absent LCP, with smectic layer scattering marked in orange, and field direction as indicated. (C, D) Scattering pattern of non-field-aligned MoS_2-containing (C) and absent (D) LCP. (E) Azimuthal profile of scattering from (top) MoS_2 aligned under 6 T (red) and 0 T (black) magnetic fields and (bottom) LCP aligned under 6 T (orange) and 0 T (black) magnetic fields. The color in each plot matches the circular-colored regions in panels A and B.

degeneracy of the nanosheets. The condition that the sheet surface normal be perpendicular to the field can be satisfied by any orientation of the surface normal in the plane perpendicular to the field direction, such that the surface normal is degenerate around the magnetic field direction (Figure 1).

The magnetic alignment of the 2D-MoS_2 results in optical anisotropy that is detectable in measurements on ensembles of nanosheets. We performed Raman measurements of magnetically aligned MoS_2 with the incident light parallel to the applied field direction and calculated the ratio L of the integrated peak intensities for the A_{1g} and E^1_{2g} modes. For field aligned sheets, the A_{1g}/E^1_{2g} intensity ratio observed was L_B = 2.0 ± 0.1, which is broadly consistent with prior reports regarding vertically aligned nanosheets with vertically incident light.[20,21] This ratio is higher than that for randomly oriented nonaligned sample, L_0 = 1.5 ± 0.4 (see Figure 4A). The ratio L_B/L_0 can be compared to theoretical estimates, derived by using a symmetry-reduced form of the Raman tensor for MoS_2,[25] which are quantitatively related to the coefficient of the second-order Legendre polynomial, $P_2\langle\cos\theta\rangle$, that describes the orientation distribution of the nanosheet surface normal with respect to the magnetic field (details in the Supporting Information). For perfectly aligned nanosheets with surface normal orthogonal to the field, $P_2\langle\cos\theta\rangle = -1/2$, and we anticipate $L_B/L_0 = 2$. Our experimental results, L_B/L_0 = 4/3, indicate that the field-processed nanosheets are clearly aligned relative to non-field-processed samples, though less than perfectly so, with $P_2\langle\cos\theta\rangle = -1/5$.

The difference in intensities for aligned versus nonaligned samples originates due to differential excitation of the A_{1g} relative to the E^1_{2g} Raman modes; the A_{1g} vibrations are out-of-plane while E^1_{2g} are in-plane, relative to the nanosheets[56] (see Figure 4B). The surface normals of the magnetically aligned nanosheets are perpendicular to the incident light. In addition, we examined the distribution of the intensity ratio determined from multiple measurements at different locations on aligned samples. The intensity ratio distribution was broader for nonaligned samples compared to aligned samples. This originates due to the fact that nonaligned samples contain an orientation-mixed population of nanosheets. Micrometer-scale local sampling during Raman characterization therefore leads to a large variance in the intensity ratio. By contrast, the more tightly distributed nanosheet orientation in magnetically aligned samples leads to a lower variance (Figure 4C).

Optical anisotropy was also observed in the PL emission (Figure 4D,E). In magnetically aligned samples, the optical signal from the nanosheets is enhanced when the incident light is perpendicular to the field direction, compared to the case where it is parallel to it, with an intensity ratio $I_{B\perp k}/I_{B\parallel k}$ of 1.30 ± 0.08, measured at the ∼635 nm PL emission peak. This ratio was 0.99 ± 0.06 for nonaligned samples, indicating no preferential orientation-dependent emission. Recent studies of visible and near-infrared birefringence in MoS_2 highlight the disparate contributions of intralayer (i.e., in-plane) versus interlayer (i.e., out-of-plane) excitons in photon absorption.[6] Similarly, PL anisotropy is related to the dominant contribution of in-plane relative to out-of-plane excitonic dipoles.[57,58] For the magnetically aligned MoS_2 nanosheets, when the incident light is parallel to the magnetic field (k_z and B_z, see Figure 4D), the electrical field associated with propagating photons oscillates in the xy plane and statistically

https://doi.org/10.1021/acs.jpclett.2c01819
J. Phys. Chem. Lett. 2022, 13, 7994−8001

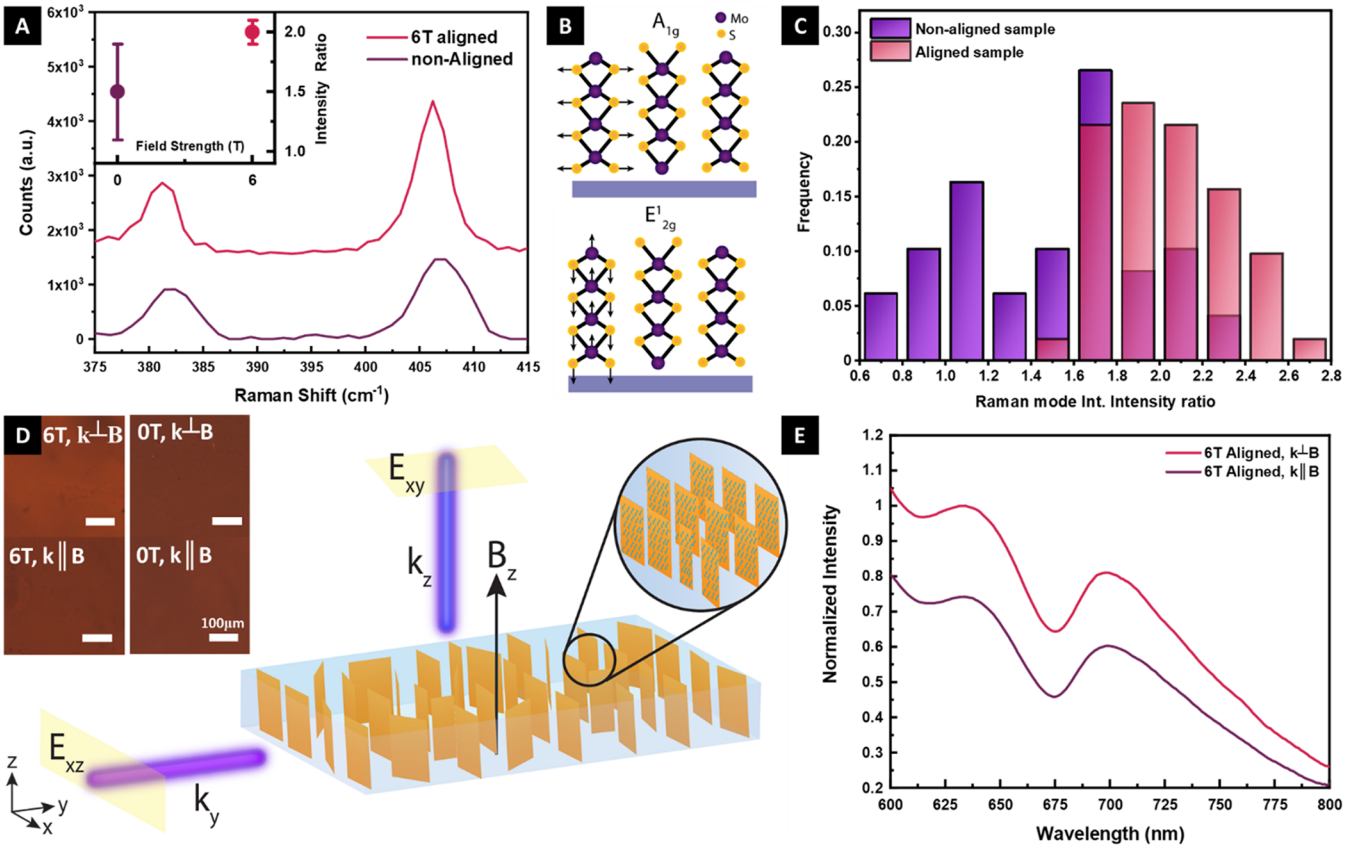

Figure 4. Optical anisotropy from field aligned LCP-embedded MoS_2 nanosheets. (A) Raman measurements of field-aligned and non-field-aligned samples. Inset: average experimental Raman mode integrated intensity ratio at different field strengths. (B) Schematic illustration of the A_{1g} and E^1_{2g} Raman modes in vertically aligned MoS_2 nanosheets. (C) Distributions of Raman A_{1g} and E^1_{2g} Raman modes integrated intensity ratios for nonaligned and a magnetically aligned samples. (D) Schematic depicting the measurement methodology, with incident light hitting the sample parallel and perpendicular to the magnetic field direction. Inset: fluorescent microscopy images of field-aligned and nonaligned MoS_2-containing LCP samples, with different incident light and magnetic field directions relations, as indicated. All scale bars represent 100 μm. (E) Direct PL measurement of field aligned LCP-embedded MoS_2 nanosheets with incident light perpendicular and parallel to the magnetic field direction.

samples in-plane and out-of-plane contributions equally. Conversely, for light incident perpendicular to the magnetic field (k_y, see Figure 4D), the out-of-plane contribution is sampled less frequently, by a factor of 2.

The orientation-dependent PL intensity ratio can be directly visualized by using fluorescence microscopy (Figure 4D, inset). Several field-aligned and non-field-aligned samples were imaged, and the fluorescence intensity ratio was calculated via image analysis that integrated individual pixel intensities. The results were in good agreement with the direct PL measurements, with $I_{B\perp k}/I_{B\parallel k}$ of 1.20 ± 0.09 and 0.97 ± 0.04 for magnetically aligned and nonaligned-samples, respectively. The results of PL anisotropy can be used to provide a lower bound estimate for the relative intensity of in-plane versus out-of-plane contributions to MoS_2 emission, that is, the fluorescence dichroic ratio. The calculation (details in the Supporting Information) assumes that PL sampling has occurred over statistically representative ensembles and that the nanosheets are perfectly aligned in the field-aligned case and perfectly random for the nonaligned situation. For this reason, i.e., the assumption of perfectly aligned versus perfectly random, the estimate is a lower bound on the dichroic ratio as a larger such ratio would be needed to satisfactorily account for the observed PL anisotropy in the case of less than perfect alignment, as suggested by the Raman results.

We use the average intensity ratio from the PL and direct imaging experiments, $I_{B\perp k}/I_{B\parallel k}$ = 1.25, and that the dichroic ratio for in-plane vs out-out-plane emission is IP/OP = 3. This represents the first experimental estimate of this property for ensembles of suspended MoS_2 nanosheets, highlighting the potential of the presented alignment technique in furthering the study of anisotropic properties of few-layer MoS_2. Knowledge of the dichroic ratio can provide a simple means of assessing the orientation distribution coefficient of ensembles of MoS_2 nanosheets in relevant scenarios.

In conclusion, we present a methodology to orient MoS_2 nanosheets using the magnetic field response of a LCP in which the nanosheets are individually suspended, which allows to reveal the optical anisotropy originating from ensembles of such oriented MoS_2. The coupling between the alignment of the nanosheets and the LCP is governed by the planar anchoring condition of the mesogens at the MoS_2 basal plane. Raman spectroscopy and PL measurements reflect the orientational order present in the system as seen from the intensity ratio of A_{1g} and E^1_{2g} vibrational modes and emission anisotropy, respectively. The emission data provided a rough estimate for the relative contributions of in-plane versus out-of-plane excitonic dipoles of MoS_2. The ability to preferentially orient MoS_2 nanosheets, as discussed here, provides new opportunities for studying anisotropic properties of MoS_2 over statistically relevant numbers of nanosheets and free of

https://doi.org/10.1021/acs.jpclett.2c01819
J. Phys. Chem. Lett. 2022, 13, 7994−8001

potential substrate-induced effects. While the approach used here was focused on few-layer MoS_2, appropriate optimization of the exfoliation process can be advanced readily yield single-layer nanosheets, which we expect will be similarly dispersed and aligned as shown for few-layer nanosheets. In addition, we anticipate that the technique demonstrated here presents a new pathway to harness the intrinsic anisotropy of individually dispersed MoS_2 nanosheets in emerging technologies and photonic applications.

■ ASSOCIATED CONTENT

Supporting Information

The Supporting Information is available free of charge at https://pubs.acs.org/doi/10.1021/acs.jpclett.2c01819.

Experimental and computational methods; differential calorimetry data for polymerized RM105; room temperature and temperature resolved 1D small-angle X-ray scattering data; photographs of polymerized RM105 dispersed MoS_2; numerical calculations data (PDF)

■ AUTHOR INFORMATION

Corresponding Author

Chinedum O. Osuji − *Department of Chemical and Biomolecular Engineering, University of Pennsylvania, Philadelphia, Pennsylvania 19104, United States; Department of Chemical and Environmental Engineering, Yale University, New Haven, Connecticut 06511, United States;* orcid.org/0000-0003-0261-3065; Email: cosuji@seas.upenn.edu

Authors

Uri R. Gabinet − *Department of Chemical and Biomolecular Engineering, University of Pennsylvania, Philadelphia, Pennsylvania 19104, United States; Department of Chemical and Environmental Engineering, Yale University, New Haven, Connecticut 06511, United States*

Changyeon Lee − *Department of Chemical and Biomolecular Engineering, University of Pennsylvania, Philadelphia, Pennsylvania 19104, United States*

Na Kyung Kim − *Department of Chemical and Biomolecular Engineering, University of Pennsylvania, Philadelphia, Pennsylvania 19104, United States*

Martin Hulman − *Institute of Electrical Engineering, Slovak Academy of Sciences, 84104 Bratislava, Slovakia;* orcid.org/0000-0002-5598-9245

Sarah M. Thompson − *Department of Electrical and Systems Engineering, University of Pennsylvania, Philadelphia, Pennsylvania 19104, United States*

Cherie R. Kagan − *Department of Electrical and Systems Engineering, Department of Materials Science and Engineering, and Department of Chemistry, University of Pennsylvania, Philadelphia, Pennsylvania 19104, United States;* orcid.org/0000-0001-6540-2009

Complete contact information is available at: https://pubs.acs.org/10.1021/acs.jpclett.2c01819

Notes

The authors declare no competing financial interest.

■ ACKNOWLEDGMENTS

This work was supported by NSF through DMR (1720530, 1945966). The authors acknowledge the use of Dual Source and Environmental X-ray scattering facility operated by the Laboratory for Research on the Structure of Matter at the University of Pennsylvania (NSF DMR1720530). The equipment purchase was made possible by NSF MRI grant (1725969), ARO DURIP grant (W911NF-17-1-0282), and the University of Pennsylvania. M.H. acknowledges a support from the project APVV-19-0365. The authors thank Dr. Deep Jariwala for insightful discussions concerning electronic and optical properties of MoS_2 nanosheets. The Authors would like to thank Dr. Gilad Kaufman for his useful input and suggestions on figure organization.

■ ABBREVIATIONS

LC, liquid crystal; LCP, liquid crystal polymer; LCE, liquid crystal elastomer; TMDs, transition-metal dichalcogenides; AFM, atomic force microscopy; DLS, dynamic light scattering; PDI, polydispersity index; DSC, differential scanning calorimetry.

■ REFERENCES

(1) Donarelli, M.; Ottaviano, L. 2D Materials for Gas Sensing Applications: A Review on Graphene Oxide, MoS2, WS2 and Phosphorene. *Sensors* **2018**, *18*, 3638.

(2) Mak, K. F.; Lee, C.; Hone, J.; Shan, J.; Heinz, T. F. Atomically Thin MoS_2: A New Direct-Gap Semiconductor. *Phys. Rev. Lett.* **2010**, *105*, 136805.

(3) Venkata Subbaiah, Y. P.; Saji, K. J.; Tiwari, A. Atomically Thin MoS2: A Versatile Nongraphene 2D Material. *Adv. Funct. Mater.* **2016**, *26*, 2046−2069.

(4) Wang, H.; Li, C.; Fang, P.; Zhang, Z.; Zhang, J. Z. Synthesis, properties, and optoelectronic applications of two-dimensional MoS2 and MoS2-based heterostructures. *Chem. Soc. Rev.* **2018**, *47*, 6101−6127.

(5) Rasamani, K. D.; Alimohammadi, F.; Sun, Y. Interlayer-expanded MoS2. *Mater. Today* **2017**, *20*, 83−91.

(6) Ermolaev, G. A.; Grudinin, D. V.; Stebunov, Y. V.; Voronin, K. V.; Kravets, V. G.; Duan, J.; Mazitov, A. B.; Tselikov, G. I.; Bylinkin, A.; Yakubovsky, D. I.; Novikov, S. M.; Baranov, D. G.; Nikitin, A. Y.; Kruglov, I. A.; Shegai, T.; Alonso-González, P.; Grigorenko, A. N.; Arsenin, A. V.; Novoselov, K. S.; Volkov, V. S. Giant optical anisotropy in transition metal dichalcogenides for next-generation photonics. *Nat. Commun.* **2021**, *12*, 854.

(7) Coleman, J. N.; Lotya, M.; O'Neill, A.; Bergin, S. D.; King, P. J.; Khan, U.; Young, K.; Gaucher, A.; De, S.; Smith, R. J.; Shvets, I. V.; Arora, S. K.; Stanton, G.; Kim, H.-Y.; Lee, K.; Kim, G. T.; Duesberg, G. S.; Hallam, T.; Boland, J. J.; Wang, J. J.; Donegan, J. F.; Grunlan, J. C.; Moriarty, G.; Shmeliov, A.; Nicholls, R. J.; Perkins, J. M.; Grieveson, E. M.; Theuwissen, K.; McComb, D. W.; Nellist, P. D.; Nicolosi, V. Two-Dimensional Nanosheets Produced by Liquid Exfoliation of Layered Materials. *Science* **2011**, *331*, 568−571.

(8) Lopez-Sanchez, O.; Lembke, D.; Kayci, M.; Radenovic, A.; Kis, A. Ultrasensitive photodetectors based on monolayer MoS2. *Nat. Nanotechnol.* **2013**, *8*, 497−501.

(9) Backes, C.; Smith, R. J.; McEvoy, N.; Berner, N. C.; McCloskey, D.; Nerl, H. C.; O'Neill, A.; King, P. J.; Higgins, T.; Hanlon, D.; Scheuschner, N.; Maultzsch, J.; Houben, L.; Duesberg, G. S.; Donegan, J. F.; Nicolosi, V.; Coleman, J. N. Edge and confinement effects allow in situ measurement of size and thickness of liquid-exfoliated nanosheets. *Nat. Commun.* **2014**, *5*, 4576.

(10) Shen, J.; He, Y.; Wu, J.; Gao, C.; Keyshar, K.; Zhang, X.; Yang, Y.; Ye, M.; Vajtai, R.; Lou, J.; Ajayan, P. M. Liquid Phase Exfoliation of Two-Dimensional Materials by Directly Probing and Matching Surface Tension Components. *Nano Lett.* **2015**, *15*, 5449−5454.

(11) Eda, G.; Yamaguchi, H.; Voiry, D.; Fujita, T.; Chen, M.; Chhowalla, M. Photoluminescence from Chemically Exfoliated MoS2. *Nano Lett.* **2011**, *11*, 5111−5116.

(12) Tian, R.; Jia, X.; Lan, M.; Wang, S.; Li, Y.; Yang, J.; Shao, D.; Feng, L.; Su, Q.; Song, H. Ionic Liquid Crystals Confining Ultrathin MoS2 Nanosheets: A High-Concentration and Stable Aqueous Dispersion. *ACS Sustain. Chem. Eng.* **2022**, *10*, 4186−4197.
(13) Wang, K.; Wang, J.; Fan, J.; Lotya, M.; O'Neill, A.; Fox, D.; Feng, Y.; Zhang, X.; Jiang, B.; Zhao, Q.; Zhang, H.; Coleman, J. N.; Zhang, L.; Blau, W. J. Ultrafast Saturable Absorption of Two-Dimensional MoS2 Nanosheets. *ACS Nano* **2013**, *7*, 9260−9267.
(14) Li, G.; Zhang, D.; Qiao, Q.; Yu, Y.; Peterson, D.; Zafar, A.; Kumar, R.; Curtarolo, S.; Hunte, F.; Shannon, S.; Zhu, Y.; Yang, W.; Cao, L. All The Catalytic Active Sites of MoS2 for Hydrogen Evolution. *J. Am. Chem. Soc.* **2016**, *138*, 16632−16638.
(15) Chen, S.; Sood, A.; Pop, E.; Goodson, K. E.; Donadio, D. Strongly tunable anisotropic thermal transport in MoS2 by strain and lithium intercalation: first-principles calculations. *2D Materials* **2019**, *6*, 025033.
(16) Huang, T.-X.; Cong, X.; Wu, S.-S.; Lin, K.-Q.; Yao, X.; He, Y.-H.; Wu, J.-B.; Bao, Y.-F.; Huang, S.-C.; Wang, X.; Tan, P.-H.; Ren, B. Probing the edge-related properties of atomically thin MoS2 at nanoscale. *Nat. Commun.* **2019**, *10*, 5544.
(17) Hu, D.; Yang, X.; Li, C.; Liu, R.; Yao, Z.; Hu, H.; Corder, S. N. G.; Chen, J.; Sun, Z.; Liu, M.; Dai, Q. Probing optical anisotropy of nanometer-thin van der waals microcrystals by near-field imaging. *Nat. Commun.* **2017**, *8*, 1471.
(18) Singh, A.; Jo, S. S.; Li, Y.; Wu, C.; Li, M.; Jaramillo, R. Refractive Uses of Layered and Two-Dimensional Materials for Integrated Photonics. *ACS Photonics* **2020**, *7*, 3270−3285.
(19) Kumar, D.; Singh, B.; Kumar, R.; Kumar, M.; Kumar, P. Anisotropic electron-photon-phonon coupling in layered MoS_2. *J. Phys.: Condens. Matter* **2020**, *32*, 415702.
(20) Kong, D.; Wang, H.; Cha, J. J.; Pasta, M.; Koski, K. J.; Yao, J.; Cui, Y. Synthesis of MoS2 and MoSe2 Films with Vertically Aligned Layers. *Nano Lett.* **2013**, *13*, 1341−1347.
(21) Bolhuis, M.; Hernandez-Rueda, J.; van Heijst, S. E.; Tinoco Rivas, M.; Kuipers, L.; Conesa-Boj, S. Vertically-oriented MoS2 nanosheets for nonlinear optical devices. *Nanoscale* **2020**, *12*, 10491−10497.
(22) Camellini, A.; Mennucci, C.; Cinquanta, E.; Martella, C.; Mazzanti, A.; Lamperti, A.; Molle, A.; de Mongeot, F. B.; Della Valle, G.; Zavelani-Rossi, M. Ultrafast Anisotropic Exciton Dynamics in Nanopatterned MoS2 Sheets. *ACS Photonics* **2018**, *5*, 3363−3371.
(23) Mennucci, C.; Mazzanti, A.; Martella, C.; Lamperti, A.; Bhatnagar, M.; Lo Savio, R.; Repetto, L.; Camellini, A.; Zavelani-Rossi, M.; Molle, A.; Buatier de Mongeot, F.; Della Valle, G. Geometrical Engineering of Giant Optical Dichroism in Rippled MoS2 Nanosheets. *Adv. Opt. Mater.* **2021**, *9*, 2001408.
(24) Martella, C.; Ortolani, L.; Cianci, E.; Lamperti, A.; Morandi, V.; Molle, A. Large-area patterning of substrate-conformal MoS2 nanotrenches. *Nano Res.* **2019**, *12*, 1851−1854.
(25) Hulman, M.; Sojková, M.; Végsö, K.; Mrkyvkova, N.; Hagara, J.; Hutár, P.; Kotrusz, P.; Hudec, J.; Tokár, K.; Majkova, E.; Siffalovic, P. Polarized Raman Reveals Alignment of Few-Layer MoS2 Films. *J. Phys. Chem. C* **2019**, *123*, 29468−29475.
(26) Maduro, L.; Noordam, M.; Bolhuis, M.; Kuipers, L.; Conesa-Boj, S. Position-Controlled Fabrication of Vertically Aligned Mo/MoS2 Core-Shell Nanopillar Arrays. *Adv. Funct. Mater.* **2022**, *32*, 2107880.
(27) Shen, W.; Wei, Y.; Hu, C.; López-Posadas, C. B.; Hohage, M.; Sun, L. Substrate Induced Optical Anisotropy in Monolayer MoS2. *J. Phys. Chem. C* **2020**, *124*, 15468−15473.
(28) Kotova, L. V.; Rakhlin, M. V.; Galimov, A. I.; Eliseyev, I. A.; Borodin, B. R.; Platonov, A. V.; Kirilenko, D. A.; Poshakinskiy, A. V.; Shubina, T. V. MoS2 flake as a van der Waals homostructure: luminescence properties and optical anisotropy. *Nanoscale* **2021**, *13*, 17566−17575.
(29) Gabinet, U. R.; Lee, C.; Poling-Skutvik, R.; Keane, D.; Kim, N. K.; Dong, R.; Vicars, Z.; Cai, Y.; Thosar, A. U.; Grun, A.; Thompson, S. M.; Patel, A. J.; Kagan, C. R.; Composto, R. J.; Osuji, C. O. Nanocomposites of 2D-MoS2 Exfoliated in Thermotropic Liquid Crystals. *ACS Mater. Lett.* **2021**, *3*, 704−712.
(30) Splendiani, A.; Sun, L.; Zhang, Y.; Li, T.; Kim, J.; Chim, C.-Y.; Galli, G.; Wang, F. Emerging Photoluminescence in Monolayer MoS2. *Nano Lett.* **2010**, *10*, 1271−1275.
(31) McCreary, K. M.; Hanbicki, A. T.; Sivaram, S. V.; Jonker, B. T. A- and B-exciton photoluminescence intensity ratio as a measure of sample quality for transition metal dichalcogenide monolayers. *APL Materials* **2018**, *6*, 111106.
(32) Chu, X. S.; Yousaf, A.; Li, D. O.; Tang, A. A.; Debnath, A.; Ma, D.; Green, A. A.; Santos, E. J. G.; Wang, Q. H. Direct Covalent Chemical Functionalization of Unmodified Two-Dimensional Molybdenum Disulfide. *Chem. Mater.* **2018**, *30*, 2112−2128.
(33) Chow, P. K.; Jacobs-Gedrim, R. B.; Gao, J.; Lu, T.-M.; Yu, B.; Terrones, H.; Koratkar, N. Defect-Induced Photoluminescence in Monolayer Semiconducting Transition Metal Dichalcogenides. *ACS Nano* **2015**, *9*, 1520−1527.
(34) Akselrod, G. M.; Ming, T.; Argyropoulos, C.; Hoang, T. B.; Lin, Y.; Ling, X.; Smith, D. R.; Kong, J.; Mikkelsen, M. H. Leveraging Nanocavity Harmonics for Control of Optical Processes in 2D Semiconductors. *Nano Lett.* **2015**, *15*, 3578−3584.
(35) Huang, J.; Akselrod, G. M.; Ming, T.; Kong, J.; Mikkelsen, M. H. Tailored Emission Spectrum of 2D Semiconductors Using Plasmonic Nanocavities. *ACS Photonics* **2018**, *5*, 552−558.
(36) Kinkhabwala, A.; Yu, Z.; Fan, S.; Avlasevich, Y.; Müllen, K.; Moerner, W. E. Large single-molecule fluorescence enhancements produced by a bowtie nanoantenna. *Nat. Photonics* **2009**, *3*, 654−657.
(37) Mak, K. F.; He, K.; Lee, C.; Lee, G. H.; Hone, J.; Heinz, T. F.; Shan, J. Tightly bound trions in monolayer MoS2. *Nat. Mater.* **2013**, *12*, 207−211.
(38) Li, H.; Zhang, Q.; Yap, C. C. R.; Tay, B. K.; Edwin, T. H. T.; Olivier, A.; Baillargeat, D. From Bulk to Monolayer MoS2: Evolution of Raman Scattering. *Adv. Funct. Mater.* **2012**, *22*, 1385−1390.
(39) Yu, X.; Prévot, M. S.; Sivula, K. Multiflake Thin Film Electronic Devices of Solution Processed 2D MoS2 Enabled by Sonopolymer Assisted Exfoliation and Surface Modification. *Chem. Mater.* **2014**, *26*, 5892−5899.
(40) Ahmad, R.; Srivastava, R.; Yadav, S.; Singh, D.; Gupta, G.; Chand, S.; Sapra, S. Functionalized Molybdenum Disulfide Nanosheets for 0D-2D Hybrid Nanostructures: Photoinduced Charge Transfer and Enhanced Photoresponse. *J. Phys. Chem. Lett.* **2017**, *8*, 1729−1738.
(41) Guan, G.; Zhang, S.; Liu, S.; Cai, Y.; Low, M.; Teng, C. P.; Phang, I. Y.; Cheng, Y.; Duei, K. L.; Srinivasan, B. M.; Zheng, Y.; Zhang, Y.-W.; Han, M.-Y. Protein Induces Layer-by-Layer Exfoliation of Transition Metal Dichalcogenides. *J. Am. Chem. Soc.* **2015**, *137*, 6152−6155.
(42) Xu, B.; Piñol, R.; Nono-Djamen, M.; Pensec, S.; Keller, P.; Albouy, P.-A.; Lévy, D.; Li, M.-H. Self-assembly of liquid crystal block copolymer PEG-b-smectic polymer in pure state and in dilute aqueous solution. *Faraday Discuss.* **2009**, *143*, 235−250.
(43) Noirez, L.; Keller, P.; Cotton, J. P. On the structure and the chain conformation of side-chain liquid crystal polymers. *Liq. Cryst.* **1995**, *18*, 129−148.
(44) Davidson, P. X-ray diffraction by liquid crystalline side-chain polymers. *Prog. Polym. Sci.* **1996**, *21*, 893−950.
(45) Sano, K.; Kim, Y. S.; Ishida, Y.; Ebina, Y.; Sasaki, T.; Hikima, T.; Aida, T. Photonic water dynamically responsive to external stimuli. *Nat. Commun.* **2016**, *7*, 12559.
(46) Wang, X.; Li, X.; Aya, S.; Araoka, F.; Ishida, Y.; Kikkawa, A.; Kriener, M.; Taguchi, Y.; Ebina, Y.; Sasaki, T.; Koshiya, S.; Kimoto, K.; Aida, T. Reversible Switching of the Magnetic Orientation of Titanate Nanosheets by Photochemical Reduction and Autoxidation. *J. Am. Chem. Soc.* **2018**, *140*, 16396−16401.
(47) Lu, X.; Feng, X.; Werber, J. R.; Chu, C.; Zucker, I.; Kim, J.-H.; Osuji, C. O.; Elimelech, M. Enhanced antibacterial activity through the controlled alignment of graphene oxide nanosheets. *Proc. Natl. Acad. Sci. U. S. A.* **2017**, *114*, E9793−E9801.

https://doi.org/10.1021/acs.jpclett.2c01819
J. Phys. Chem. Lett. 2022, 13, 7994−8001

(48) Liu, Q.; Ackerman, P. J.; Lubensky, T. C.; Smalyukh, I. I. Biaxial ferromagnetic liquid crystal colloids. *Proc. Natl. Acad. Sci. U. S. A.* **2016**, *113*, 10479−10484.
(49) Liu, Q.; Senyuk, B.; Tang, J.; Lee, T.; Qian, J.; He, S.; Smalyukh, I. I. Plasmonic Complex Fluids of Nematiclike and Helicoidal Self-Assemblies of Gold Nanorods with a Negative Order Parameter. *Phys. Rev. Lett.* **2012**, *109*, 088301.
(50) Rokhlenko, Y.; Gopinadhan, M.; Osuji, C. O.; Zhang, K.; O'Hern, C. S.; Larson, S. R.; Gopalan, P.; Majewski, P. W.; Yager, K. G. Magnetic Alignment of Block Copolymer Microdomains by Intrinsic Chain Anisotropy. *Phys. Rev. Lett.* **2015**, *115*, 258302.
(51) Majewski, P. W.; Osuji, C. O. Non-degenerate magnetic alignment of self-assembled mesophases. *Soft Matter* **2009**, *5*, 3417−3421.
(52) Kim, D. W.; Ok, J. M.; Jung, W.-B.; Kim, J.-S.; Kim, S. J.; Choi, H. O.; Kim, Y. H.; Jung, H.-T. Direct Observation of Molybdenum Disulfide, MoS2, Domains by Using a Liquid Crystalline Texture Method. *Nano Lett.* **2015**, *15*, 229−234.
(53) Hara, M.; Iwakabe, Y.; Tochigi, K.; Sasabe, H.; Garito, A. F.; Yamada, A. Anchoring structure of smectic liquid-crystal layers on MoS2 observed by scanning tunnelling microscopy. *Nature* **1990**, *344*, 228−230.
(54) Lacaze, E.; Apicella, A.; De Santo, M. P.; Coursault, D.; Alba, M.; Goldmann, M.; Barberi, R. Ordered interfaces for dual easy axes in liquid crystals. *Soft Matter* **2011**, *7*, 1078−1083.
(55) Lacaze, E.; Michel, J. P.; Goldmann, M.; Gailhanou, M.; Boissieu, M. d.; Alba, M. Bistable nematic and smectic anchoring in the liquid crystal octylcyanobiphenyl (8CB) adsorbed on a MoS_2 single crystal. *Phys. Rev. E* **2004**, *69*, 041705.
(56) Verble, J. L.; Wieting, T. J. Lattice Mode Degeneracy in MoS_2 and Other Layer Compounds. *Phys. Rev. Lett.* **1970**, *25*, 362−365.
(57) Schuller, J. A.; Karaveli, S.; Schiros, T.; He, K.; Yang, S.; Kymissis, I.; Shan, J.; Zia, R. Orientation of luminescent excitons in layered nanomaterials. *Nat. Nanotechnol.* **2013**, *8*, 271−276.
(58) Liang, W. Y. Optical anisotropy in layer compounds. *J. Phys.: Condens. Matter* **1973**, *6*, 551−565.

https://doi.org/10.1021/acs.jpclett.2c01819
J. Phys. Chem. Lett. 2022, 13, 7994−8001